Volume 5 | Number 16 | 28 April 2017 | Pages 2859–3060

Journal of Materials Chemistry B

Materials for biology and medicine

rsc.li/materials-b

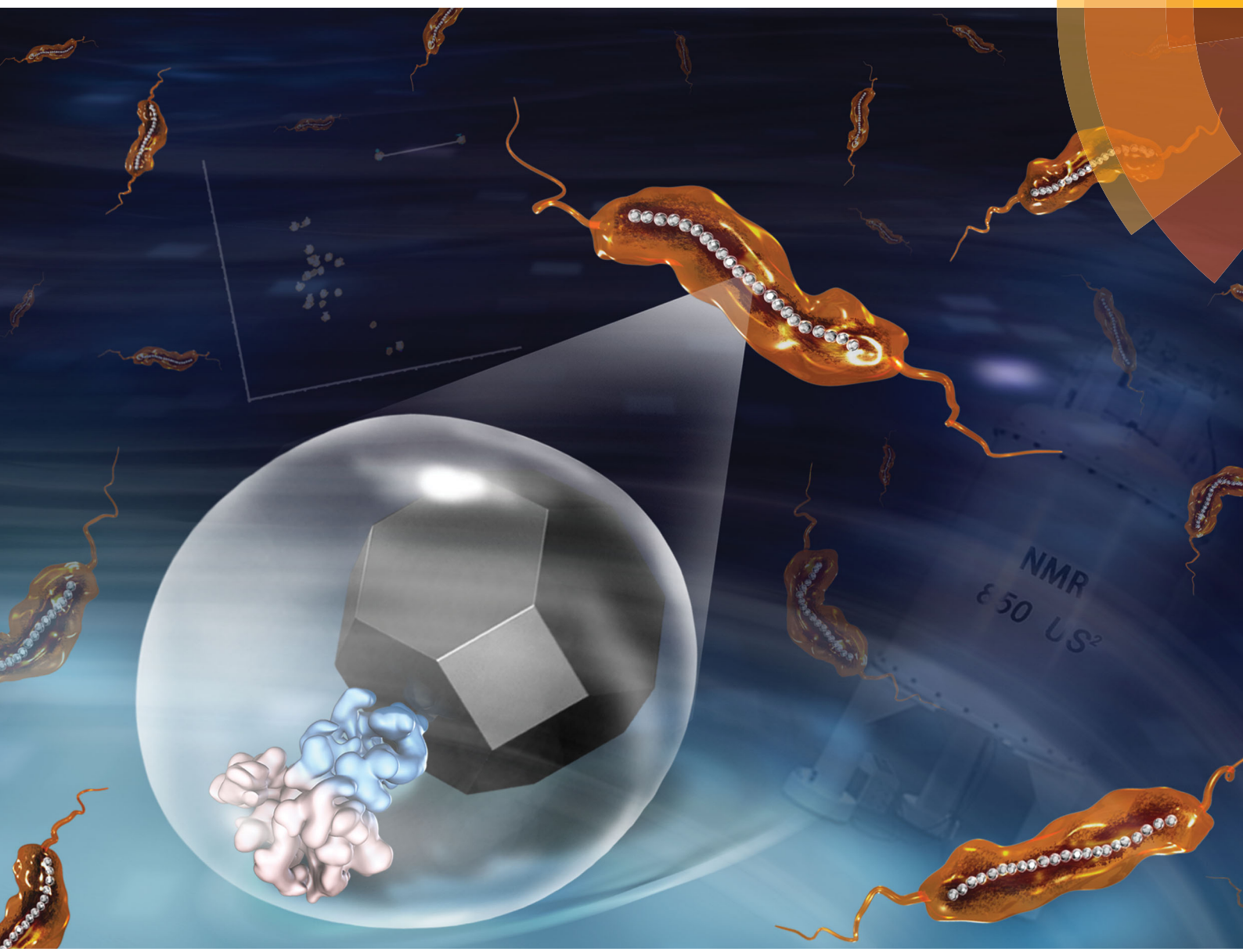

ISSN 2050-750X

ROYAL SOCIETY OF CHEMISTRY

PAPER

Tao Luo, Han Dai, Junfeng Wang *et al.*

NMR studies of the interactions between AMB-1 Mms6 protein and magnetosome Fe_3O_4 nanoparticles

Journal of Materials Chemistry B

PAPER

View Article Online
View Journal | View Issue

Cite this: J. Mater. Chem. B, 2017, 5, 2888

NMR studies of the interactions between AMB-1 Mms6 protein and magnetosome Fe_3O_4 nanoparticles†

Kun Ma, ‡[ab] Hongxin Zhao, ‡[abc] Xinwei Zheng, [a] Hongbin Sun, [ab] Lin Hu, [a] Lei Zhu, [ab] Yang Shen, [d] Tao Luo, *[e] Han Dai *[a] and Junfeng Wang *[abc]

Received 28th February 2017,
Accepted 17th March 2017

DOI: 10.1039/c7tb00570a

rsc.li/materials-b

Mms6 protein from *magnetotactic bacteria* strain AMB-1 is responsible for controlling the formation of magnetite nanoparticles both *in vitro* and *in vivo*. High-resolution NMR studies showed the C-terminal DEEVE motif and the following residues undergoing conformation change upon magnetosome Fe_3O_4 crystal binding. The N-terminal hydrophobic packing of Mms6 protein is important for arranging the DEEVE motifs into a correct assembly and orientation that are crucial for magnetite crystal recognition.

1 Introduction

The formation of highly ordered inorganic materials with complex form is a widespread biological phenomenon called biomineralization and occurs in almost all groups of organisms from prokaryotes (*e.g.*, magnetite nanocrystals in certain bacteria) to humans (bone and teeth).[1–6] The *Magnetospirillum magneticum* AMB-1 is a *magnetotactic bacterium* that contains magnetite-filled magnetosomes and migrates along the geomagnetic field lines. *M. magneticum* also contributes to the global iron cycle by actively converting iron to magnetite or greigite nanoparticles within magnetosomes.[6–9] Mms6 protein, a magnetosome-associated protein from *M. magneticum* AMB-1 has been classified as an important member of the magnetite (Fe_3O_4) biomineralization mechanism.[10–13] In addition, Mms6 promotes the formation of Fe_3O_4 magnetic nanoparticles (MNPs) with uniform size and morphology through *in vitro* chemical synthesis.[10,14–19]

After Mms6 was first reported by A. Arakaki *et al.*[10] in 2003, this protein was extensively studied. Mms6 comprises a hydrophobic N-terminal region and a hydrophilic C-terminal region. This amphiphilic feature orients Mms6 in a way that its N-terminal interacts with magnetosome membranes while the hydrophilic C-terminal faces the magnetosome interior. In aqueous solution, purified Mms6 self-assembles into micellar structures.[20,21] These large aggregates are able to bind and accumulate ferric ions from solution,[22–24] and magnetite was reported to form in the presence of Mms6 protein micelles.[10,14,25] The cytoplasmic domain of Mms6 alone exhibits some characteristics similar to those of the full-length protein, such as iron binding and a limited ability to affect magnetite crystal growth.[16,26,27] Various biophysical techniques, such as size-exclusion chromatography,[20,21] dynamic light scattering,[20] liquid cell TEM,[23] small-angle X-ray scattering,[22] as well as TEM with dried samples,[21] have been applied to study the protein assembly and ion-bindings of full-length Mms6 and Mms6 derived peptides. A recent NMR study by A. E. Rawlings *et al.*[28] studied the interaction between the Mms6 C-terminal peptide and Fe^{2+}, demonstrating the advantages of high-resolution NMR in providing structural information at atomic resolution. However, how the full-length Mms6 functions both *in vivo* and *in vitro* is still poorly understood, especially how Mms6 interacts with various iron oxides and iron oxyhydroxides, specifically the magnetosome magnetite nanocrystals. To a great extent, the amphiphile and the self-assembly feature of Mms6 have limited the application of techniques like protein crystallization and high-resolution NMR. In this study, we utilized the high-resolution NMR technique to characterize full-length Mms6 and its C-terminal 25-residue fragment (Mms6C25) (Fig. 1a), and to study the interaction with Magnetosome Fe_3O_4 nanoparticles.

2 Experimental section

Mms6 protein expression and purification

His6–Mms6 fusion protein was expressed and purified as described previously.[10,17] Briefly, the overnight grown LB culture

[a] High Magnetic Field Laboratory, Chinese Academy of Sciences, Hefei 230031, Anhui, P. R. China. E-mail: junfeng@hmfl.ac.cn, daihan@hmfl.ac.cn
[b] Key Laboratory of High Magnetic Field and Ion Beam Physical Biology, Chinese Academy of Sciences, Hefei 230031, Anhui, P. R. China
[c] University of Science and Technology of China, Hefei 230036, Anhui, P. R. China
[d] Laboratory of Chemical Physics, National Institute of Diabetes and Digestive and Kidney Diseases, National Institutes of Health, Bethesda, MD 20892 0520, USA
[e] Institute of Intelligent Machines, Chinese Academy of Sciences, Hefei 230031, Anhui, P. R. China. E-mail: tluo@iim.ac.cn

† Electronic Supplementary Information (ESI) available. See DOI: 10.1039/c7tb00570a

‡ These authors contributed equally to this work.

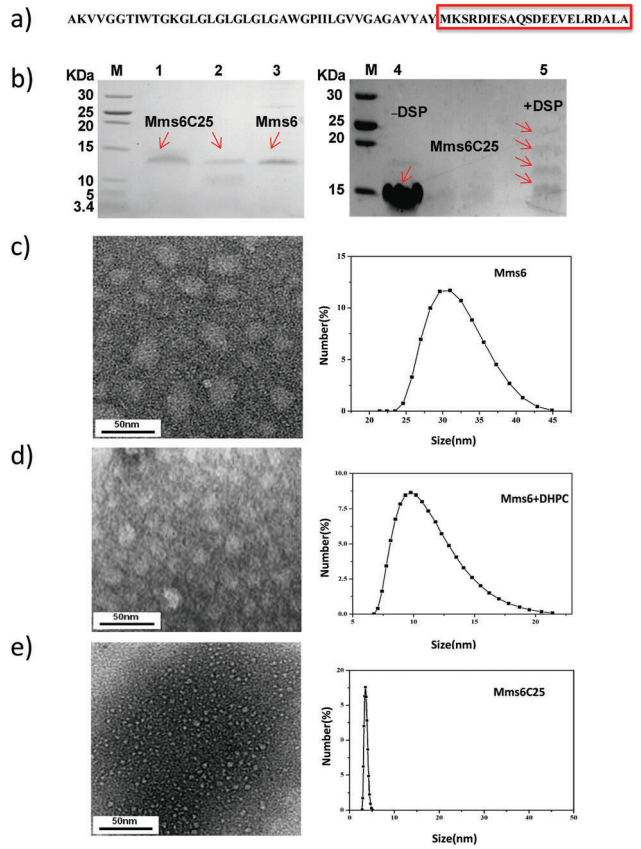

Fig. 1 Mms6 and Mms6C25 form micelle-like assembly in aqueous solutions. (a) The amino acid sequence of Mms6; the red box highlights the fragment corresponding to Mms6C25. (b) The SDS-PAGE gels of Mms6 (lane 3), Mms6C25 (lane 1 and 2), and Mms6C25 with no DSP cross-linkers (lane 4), and Mms6C25 with DSP cross-linkers (lane 5). (c) The high-resolution transmission electron microscopy (TEM) image (left) of Mms6 and the size distribution (right) measured by dynamic light scattering (DLS). (d) The TEM image (left) of Mms6 in DHPC and the corresponding size distribution measured by DLS (right). (e) The TEM image (left) of Mms6C25 and the corresponding size distribution measured by DLS (right).

was transferred into 500 mL M9 cultures (containing $^{15}NH_4Cl$ and ^{13}C-labeled glucose) and induced with 0.5 mM IPTG (final concentration) at an OD600 of 0.6. The cells continued to grow for 6 hours at 37 °C before harvesting. After sonication, the cell pellets were dissolved in 10 mL of dissolving buffer (20 mM Tris-base, 100 mM NaCl, 1% SDS W/V, pH 8.0) with the aid of a dounce homogenizer. After centrifugation at 14 000 rpm for 90 minutes, the supernatant was loaded onto a column pre-packed with Ni-NTA agarose beads (QIAGEN), and eluted with two column volumes of elution buffer (20 mM Tris-base, 100 mM NaCl, 1% SDS W/V, 300 mM imidazole, pH 8.0). Mms6 was dialyzed against dialysis buffer (20 mM Tris-base, 100 mM NaCl, pH 7.2) to remove SDS detergent.

Mms6C25 expression and purification

Similar to the expression protocol of Mms6, the overnight grown LB culture of SUMO–Mms6C25 fusion protein was transferred into 500 mL M9 culture (containing $^{15}NH_4Cl$ and ^{13}C-labeled glucose), and induced with 0.5 mM (final concentration) IPTG at an OD600 of 0.6. The cells continued to grow for 6 hours at 37 °C before harvesting. After sonication in the lysis buffer (20 mM Tris-base, 200 mM NaCl, pH 8.0), the supernatant was incubated with pre-equilibrated Ni-NTA agarose beads (QIAGEN). The column was then washed with 10 column volumes of lysis buffer, and eluted with 2 columns of elution buffer (20 mM Tris, 200 mM NaCl, 300 mM imidazole pH 8.0). The SUMO fragment was cleaved by SUMO–enzyme (1 : 100 dilution v/v) at 4 °C for 6 hours. The enzyme-treated protein solution was lyophilized and purified by reverse phase high performance liquid chromatography (RP-HPLC) on a semi-preparative C4 column (from Waters Company). The fraction containing Mms6C25 was pooled and lyophilized. The molecular weight of purified Mms6C25 was verified using an LC-mass-spectrometer.

Mms6C25 crosslinking

The Mms6C25 cross-linking was performed using dithiobis-(succinimidylpropionate) (DSP, purchased from Thermo Scientific). Aliquots of a 25% DSP (dissolved in DMSO solution) stock solution were added to Mms6C25 samples to a final concentration of 5 mM. Samples were incubated at 25 °C for 30 minutes, followed by quenching with 1 M Tris buffer (final concentration 50 mM) at pH 8.0.

Dynamic light scattering (DLS)

Dynamic light scattering experiments were carried out at 25 °C on a Malvern Zetasizer Nano ZS (Malvern, UK) equipped with a solid-state laser (100 mW, 532 nm). Mms6 and Mms6C25 samples of 0.15 mM (20 mM Tris-base, 100 mM NaCl, pH 7.2) were used for DLS measurements. A total of 30 runs were examined for one analysis with an average of three independent measurements. The normalized autocorrelation data were analyzed with the software installed in the system.

NMR spectroscopy

All NMR experiments were carried out at 25 °C on a Bruker Avance 600 MHz NMR spectrometer equipped with a CryoProbe. All NMR data were processed in NMRPipe (Delaglio *et al.*, 1995, NMRPipe: a multidimensional spectral processing system based on UNIX pipes) and analyzed using Sparky (T. D. Goddard and D. G. kneller, SPARKY3, University of California, San Francisco). For Mms6C25 backbone assignments, a NMR sample with 0.5 mM ^{15}N, ^{13}C-labeled Mms6C25 (20 mM Tris-base buffer, 100 mM NaCl, pH 7.2) was used. For Mms6 backbone assignments, a NMR sample with 0.5 mM ^{15}N,^{13}C-labeled Mms6 (20 mM Tris-HCl buffer, 100 mM NaCl, 14 mM DHPC, pH 7.2) was used. The NMR experiments recorded include: 2D-^{1}H–^{15}N HSQC, 3D-HNCACB and 3D-HN(CO)CACB. In the HNCACB experiment on the Mms6 sample containing magnetosome magnetite nanoparticles, the time domain data consisted of 1024 complex points in the t3 dimension, 40 complex points in the t2 dimension and 40 complex points in the t1 dimension. The number of scans and relaxation delay were set as 8 scans and 1.2 s, respectively.

Magnetosome MNP preparation

The AMB-1 cells were harvested by centrifugation at 8000*g* for 20 minutes. After sonication, the magnetosome component in the supernatant was immobilized and accumulated on the EP-tube wall by positioning closely to a strong neodymium magnet (0.7 T), and the supernatant together with cellular debris was discarded. The magnet pulled-down magnetosome was then washed 10 times in deionized water. Buffer containing 1% SDS was added and heated at 90 °C for 5 hours. The membrane lipids and surface-coating proteins from the magnetosome were dissolved with SDS and separated with a strong neodymium magnet (0.7 T). The magnet purified magnetosome MNPs were washed 10 times with deionized water and used for the following experiments.[29,30]

Protein binding assay to magnetosome MNPs

The purified magnetosome MNPs (about 0.1 mg) were added to protein solution (1 mg ml^{-1}) and incubated for 1 hour at room temperature. A strong neodymium magnet (0.7 T) was positioned closely to the EP-tube wall to collect the MNPs. The magnet-collected MNPs were washed and magnetically precipitated 10 times with buffer (400 mM NaCl, 10 mM Tris, pH 7.2). MNPs were then boiled in SDS loading buffer and analyzed by SDS-PAGE with silver staining.

Magnetite nanoparticle synthesis

Magnetite synthesis was performed using the room temperature co-precipitation (RTCP) method as described previously.[10,17,28,31,32] 30 mM $FeSO_4$ and 60 mM $FeCl_3$ were mixed in the presence of Mms6 or Mms6C25 (0.2 mg ml^{-1}). The reaction solution (1 ml) was sparged continuously with N_2 gas to maintain anoxic conditions. The mixture was incubated at room temperature for 5 minutes and was titrated very slowly with 0.1 N NaOH solution (6 ml per hour, approximately 2.4 ml in total) under sparging nitrogen. One hour after the titration, the reaction products were magnetically collected, washed with ultra-pure water (oxygen-free) three times, and sealed for further experiments.

Transmission electron microscopy (TEM)

MNPs were re-suspended in water, and 10 μL of this solution was transferred to a carbon-coated copper grid for TEM imaging. Crystal size distribution of MNPs was analyzed by measuring both the length and width of at least 200 crystals from TEM images. The average of the long and short axis per crystal was taken as the crystal size. Crystal sizes are reported as mean ± sample standard deviation in the mean.[16] These data were compiled into a histogram and fitted with a Gaussian distribution using Origin 8.5 software.

The negative staining protein samples were made with the single droplet procedure. In brief, protein was diluted to a final concentration of 0.1 mg ml^{-1} in protein loading buffer (20 mM Tris-HCl, pH 7.5, 50 mM NaCl). After carbon-coated EM grid deposition, standard negative staining was applied with 2% (w/v) uranyl acetate. All EM images were collected with a Philips CM200 Field Emission (FEG) TEM operated at an acceleration voltage of 200 kV with 0.24 nm point resolution, using Digital Micrograph software.

Powder X-ray diffraction (XRD)

Powder XRD analysis was performed on a Philips X'Pert diffractometer. Monochromatic X-rays were generated at 40 kV from a Cu Ka source at room temperature. Intensities were collected between $2\theta = 10^{\circ}$and 90° on a Braun position sensitive detector. The raw data were processed using Jade6.5 software.

3 Results and discussion

The objective of this study was to characterize Mms6 protein and its interaction with magnetosome Fe_3O_4 nanoparticle by high-resolution NMR. The C-terminal 25-residue fragment (Mms6C25) (Fig. 1a) was used as a control to study the potential role of the N-terminal hydrophobic fragment in Mms6 assembly and crystal surface recognition.

Characterization of Mms6 and Mms6C25 micelles

To obtain isotope-labeled NMR samples, both Mms6 and Mms6C25 were produced as recombinant proteins in *E. coli*. Mms6 was over-expressed as inclusion bodies with high yield. A few refolding strategies have been tested to purify and refold the protein. In all cases, Mms6 tends to aggregate at high concentration and attention has to be taken to avoid protein precipitation. The most efficient purification procedure we found was to dissolve Mms6 inclusion bodies in SDS detergent followed by Ni-NTA purification under denaturing conditions. The SDS was then removed by a few cycles of two-step fast dialysis and centrifugation. The purified Mms6 protein band in SDS-PAGE gel is shown in lane 3 of Fig. 1b.

The N-terminus of Mms6 protein is hydrophobic, whereas the C-terminal region is rather hydrophilic. The cytoplasmic domain of Mms6, especially the last 25 residues, has been studied extensively, and was reported to bind to Fe ions and might be the domain interacting with the Fe_3O_4 crystal surface.[16,20,28,33] In most of these studies, Mms6C25 peptide was obtained from chemical synthesis. This, however, is not cost effective; and more importantly, it is not feasible for some biophysical characterization techniques such as NMR for which complicated labeling schemes are necessary. Here again, an *E. coli* system was adopted for protein expression. Short peptides like Mms6C25 are usually toxic and tend to degrade during *E. coli* expression. Therefore, an N-terminal SUMO tag was added to avoid this problem as well as to improve the expression yields.[34] The SUMO tag was removed by protease at an introduced cleavage site between SUMO and Mms6C25. Mms6C25 after reverse phase high performance liquid chromatography (RP-HPLC) purification (Fig. S1, ESI†) gave high purity as shown in lane 1 and lane 2 of Fig. 1b, and the amino acid sequence was further verified using Mass Spectroscopy (Fig. S2, ESI†).

Both Mms6 and Mms6C25 tend to form oligomers or large aggregates in solution.[20,21] Even under the SDS denaturing conditions as shown in the SDS-PAGE gel (Fig. 1b, left), Mms6

migrates as a dimer (lane 3), while Mms6C25 presents as a higher order of oligomeric states (lane 1 and 2). SDS detergent which is considered to possess strong denaturing potential, behaves more like a lipid-like detergent and preserves some secondary structural features and oligomeric properties for both Mms6 and Mms6C25. A similar observation occurs for other hydrophobic membrane proteins like influenza M2 protein that tend to form oligomers in a native lipid environment or a lipid-mimicking detergent environment.[35,36] The SDS PAGE gel of the DSP crosslinking reaction on Mms6C25 shows multiple bands, confirming its tendency of self-assembly into higher order oligomers (lane 5 in Fig. 1b, right). The conformations of Mms6 and Mms6C25 in aqueous solution were characterized further by transmission electron microscopy (TEM) and dynamic light scattering (DLS). The negative staining TEM images show that Mms6 forms large protein micelles and the particle sizes vary from 25 to 40 nm according to the DLS data (Fig. 1c), which is consistent with previous characterization.[20,21] By adding lipid-like mild detergent DHPC, the size of Mms6 micelles can be tuned down to 10 nm (Fig. 1d), which is important for biophysical characterization techniques like high-resolution NMR. As for Mms6C25, much smaller particles formed in water as demonstrated in the TEM images. The average grain size is around 3.5 nm which is about one tenth that of Mms6, with a small size variation around 1 nm as indicated by the DLS result (Fig. 1e).

The high-resolution NMR technique is utilized to characterize the conformations of Mms6 and Mms6C25 in aqueous solution. Mms6C25 is composed of mainly hydrophilic amino acids and has good solubility in aqueous solution, which makes the NMR study rather straightforward. Fig. 2b shows the ^{1}H–^{15}N HSQC spectrum of Mms6C25 with all amide resonances assigned (shown in Fig. S4, ESI† are the strip plots from the HNCACB experiment which was acquired for Mms6C25 sequential backbone resonance assignments). Nevertheless, we were not able to obtain enough NOE restraints to calculate a well-defined structure. The C_α and C_β chemical shift analysis on Mms6C25 (not shown) indicates that this fragment is largely unstructured. Similar results have been reported in a previous proton NMR study on a shorter construct for the C-terminal 20 residues of Mms6 protein[28] as well as a small-angle X-ray scattering study.[22]

Different from Mms6C25, full-length Mms6 forms large protein aggregates as shown in the TEM images above. Liquid state NMR is capable of characterizing protein aggregates in native conformation, but the slow tumbling rate associated with the large Mms6 micelle (average size around 30 nm as shown in Fig. 1c) makes it impossible to study Mms6 by high-resolution NMR. DHPC is generally considered as a mild detergent and has been used extensively in structural and functional studies of membrane proteins.[35–37] Here, we added a 14 mM mild detergent DHPC to decrease the Mms6 aggregations while retaining the primary Mms6 conformation and its protein–protein contacts. The ^{1}H–^{15}N HSQC spectrum of the Mms6 NMR sample was collected (shown in Fig. 2a, for comparison purpose, the effect of DHPC on Mms6C25 was also verified as shown in Fig. S3 from the ESI†). Only 17 peaks appear in the

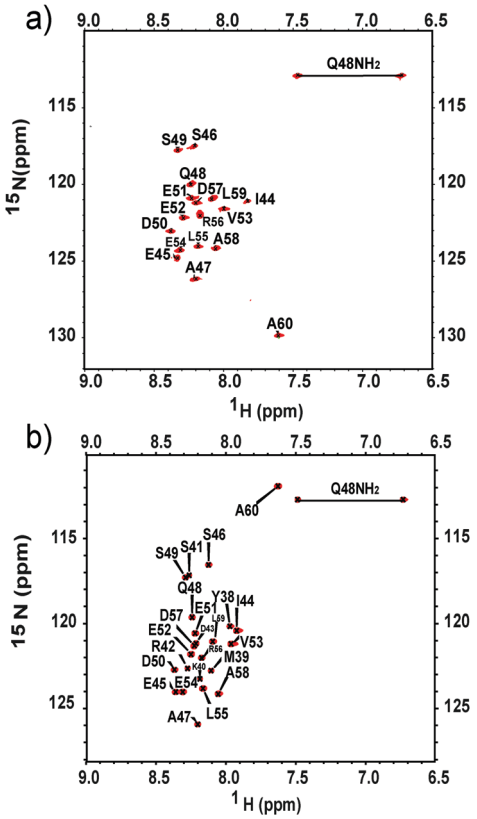

Fig. 2 The ^{1}H–^{15}N HSQC spectra and the corresponding resonance assignments of Mms6 (a) and Mms6C25 (b).

spectrum and the resonance assignments show that these peaks correspond to the last 17 residues of Mms6 from residue 44 to residue 60 (Fig. S4, ESI†). The disappearance of the N-terminal resonances is due to the fact that the N-terminal hydrophobic region of Mms6 does not adopt a homogeneous conformation in the aggregates. This observation is consistent with previous proteolytic studies that the Mms6 C-terminus is proteolytic sensitive while the N-terminus is proteolytic resistant.[20] These data support the generally accepted concept that Mms6 self-assembles into protein micelles with the C-terminal hydrophilic domain exposed to solution.[20–22]

Moreover, the observed chemical shifts of the full-length Mms6 match quite well with the corresponding resonances from the Mms6C25 spectrum. This indicates clearly that Mms6C25 and the C-terminal domain within the full-length Mms6 assembly share similar conformations in solution, and both are disordered. Intriguingly, the full-length Mms6 spectrum shows less peaks than to that of Mms6C25. Besides residues from the hydrophobic core, resonances from residues 38–43 also disappear. We proposed that this fragment of Mms6 (residues 38–43) forms a flexible linker between the hydrophobic core and the C-terminal crystal binding domain, and the corresponding NMR resonances disappear due to unfavorable local dynamics.

This hydrophobicity-driven protein packing pattern in Mms6 micelles may give hints on the packing model of Mms6 in its native magnetosome vesicle environment. The N-terminal

domain of Mms6 is likely to interact with lipid membranes and the neighbouring Mms6 molecules by hydrophobic interactions, while the hydrophilic C-terminal domain exposes to the inner magnetosome compartment and interacts with the magnetite crystal surface.

Mms6 binding to magnetosome Fe_3O_4 nanoparticles

Many studies have been carried out to study the interactions between Mms6 derived peptides and various metal ions including Fe^{2+}, Fe^{3+}, Zn^{2+}, $Ni^{2+}$and Ca^{2+}.[10,20,23,28] At low pH, Mms6 was reported to accumulate Fe^{3+} ions locally and initiate $Fe(OH)_3$ nucleation.[23] Compared to iron ion studies, nevertheless, much less is known on how Mms6 interacts with iron oxide and iron oxyhydroxide, which surpass iron ions to be the dominative species during nucleation and crystal growth. To understand the regulatory role of Mms6 during biomineralization, therefore, we went further to collect and analyze the NMR spectra of full-length Mms6 in the absence or presence of magnetosome Fe_3O_4 nanocrystals.

The interaction detail of Mms6 with magnetite crystals is the key to understand its regulatory role in biomineralization. To obtain magnetosome Fe_3O_4 nanoparticles, we cultured and harvested *M. magneticum* AMB-1 cells. After sonication, the magnetosome fraction was separated from the other cell fractions by magnetic accumulation with a strong neodymium magnet (0.7 T). The membrane lipids and coating proteins of magnetosomes were removed from magnetite crystals by SDS detergent dissolving.[29] The magnetosome MNPs obtained are mono-dispersive and homogeneous both in size and shape (Fig. 3a). To characterize protein binding to magnetosome Fe_3O_4 nanoparticles, we did a magnetic pull-down experiment. The magnetic precipitates were analyzed by SDS-PAGE with silver staining. Both Mms6 and Mms6C25 are able to bind magnetosome MNPs, while the controlling BSA protein, as expected, shows no binding to magnetosome Fe_3O_4 crystals (Fig. 3b).

Upon the titration of magnetosome Fe_3O_4 nanoparticles at pH 7.2, Mms6 resonances in the HSQC spectrum (Fig. 3c) are significantly broadened, and on average, resonance intensity decreases around 50% (Fig. S5, ESI†). This line broadening is due to the slower protein tumbling time upon Fe_3O_4 nanoparticle binding. In particular, As shown in Fig. 3c (resonance assignments details can be found in Fig. S4, ESI†), a new set of resonances from the DEEVE (residue 50–54) motif and the following residues arise indicating a different Mms6 conformation upon nanoparticle binding. The previous NMR study on the Mms6 derived peptide Mms6C20 showed that this DEEVE interacts with Fe^{2+} at neutral pH.[28] They proposed that this ferrous iron interacting property promotes the formation of magnetite in ferrous-rich solutions. For full-length Mms6 protein, our data here confirms that acidic residues, E51, E52 and E54 from the DEEVE motif, involve in magnetosome magnetite binding. Chemical shift perturbations were also observed for residues after DEEVE motifs, such as L55, R56 and A60, suggesting that these residues undergo conformation changes after magnetite binding. Unfortunately, we were not able to do a complete structural analysis at this point due to the instability of NMR samples, for which Mms6 protein precipitates together with Fe_3O_4 nanoparticles over time.

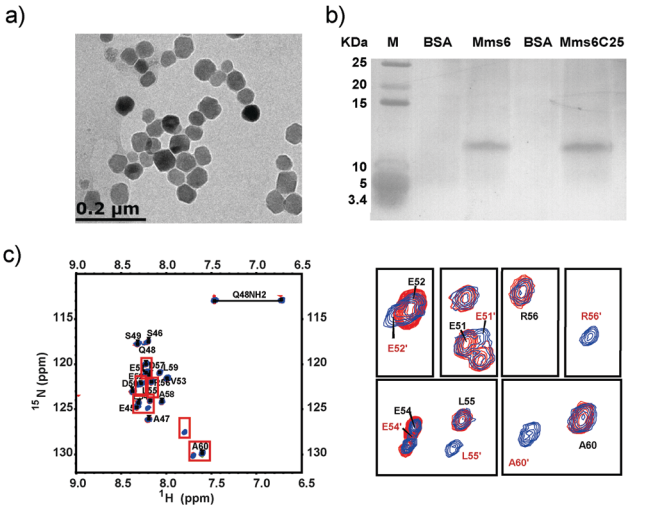

Fig. 3 The interaction between Mms6 and magnetosome Fe_3O_4 nanoparticles. (a) The TEM images of magnetosome MNPs. Membrane lipids and coated proteins were removed from magnetosome surfaces by heating and SDS treatment (left). (b) The silver staining SDS-PAGE gel of Mms6 and Mms6C25 from the magnetosome MNP pull-down experiment (right, lane 1 and 3, BSA protein control; lane 2, Mms6 protein; lane 4, Mms6C25). (c) The superimposition of the $^{1}H-^{15}N$ HSQC spectra of Mms6 in the presence (blue) and absence (red) of magnetosome Fe_3O_4 nanocrystals (left). Resonances undergo significant chemical shift perturbation (E51, E52, E54, L55, R56, and A60) were highlighted with a new set of peaks labeled as prime symbols (right).

Similar titration experiments were conducted on Mms6C25. The same line-broadening effect was observed, and the signals disappear over time due to the self-aggregation of magnetosome magnetite particles. In contrast to the Mms6 case, we did not see clear chemical shift perturbation upon Fe_3O_4 binding, except that the peak shapes are more distorted (Fig. S6, ESI†), which is an indication that the local chemical environments of nuclear spins are quite heterogeneous. Considering the fact that in solution the Mms6C25 conformation is similar to that of the C-terminal region from the intact Mms6 protein, we reason that this magnetite crystal binding difference has to be derived from regions beyond the direct protein-crystal contact interfaces. Mms6 self-aggregates into protein micelles by the N-terminal hydrophobic packing, which give rise to an ordered arrangement of the DEEVE motif that is able to support iron binding and crystallization of magnetite. Unlike Mms6, the loss of the N-terminal packing fragment makes Mms6C25 micelles easier to break. The incoherence in binding sites and binding modes impedes Mms6C25's binding specificity, although they are still able to bind MNPs nonspecifically as shown in the magnetite pull down experiment. Therefore, the MNP bound heterogeneity in Mms6C25 suggests an indispensable role of the Mms6 N-terminal domain in protein-crystal recognition.

To compare the effects of Mms6C25 and full-length Mms6 in magnetite nanoparticle growth, a room temperature

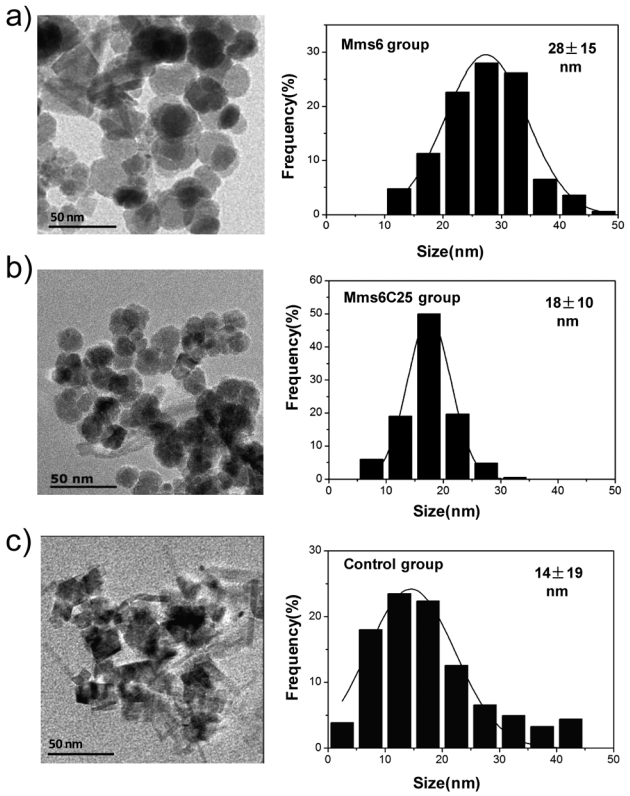

Fig. 4 TEM analysis of the magnetite nanoparticles formed by a room temperature co-precipitation method (RTCP) with or without protein. (a) In the presence of Mms6. (b) In the presence of Mms6C25. (c) In the absence of protein. Scale bars are 50 nm. MNP sizing histograms are shown with Gaussian fitting (Origin 8.5). The frequency of particles is apportioned into 5 nm bins.

co-precipitation (RTCP) method,[10,15,17] which provides relatively mild conditions for Mms6 proteins, was adopted to synthesize magnetite nanoparticles. Shown in Fig. 4a and b are the TEM pictures of nanoparticles formed in the presence of Mms6 and Mms6C25, respectively. In both cases, spherical and cubo-octahedral particles formed with a quite homogeneous size distribution, which has been observed by other groups.[14,15,19] In the presence of Mms6, the average nanoparticle size is 28 nm; for Mms6C25, smaller nanoparticles with an average size of 18 nm formed. The powder XRD analysis of the nanoparticles further verify the formation of magnetite crystals in the presence of both full-length Mms6 and Mms6C25 peptides (Fig. S8, ESI†).

As a control, magnetite particles were also synthesized in the absence of proteins. The TEM image shows a mixture of particles of various morphologies and particle sizes. Different from the spherical and cubo-octahedral magnetite particles formed in the presence of Mms6 and Mms6C25, octahedron-shaped magnetite crystals formed instead (as seen in both Fig. 4c and Fig. S7, ESI†). Moreover, some needle shaped crystals appeared which are likely to be impurities other than magnetite.[26,31,38] Besides the impurities and morphology differences, the grain size distribution is asymmetric and is skewed towards smaller sized particles. The MNPs formed in the absence of proteins are smaller (14 nm) with larger particle size variation (19 nm). The better defined crystal shapes and sizes with Mms6 and Mms6C25 may relate to the extended protein micelle surfaces and/or the protecting effects of Mms6 and Mms6C25 molecules to specific crystal surfaces.

Mms6 assembly and magnetosome magnetite crystal binding

From the above NMR study, the Mms6C25 peptide shares similar solution conformation as the C-terminal domain of the full-length Mms6 in protein micelle assembly. Nevertheless, their interaction modes with magnetosome Fe_3O_4 crystals differ significantly. Bird *et al.* reported a similar observation that Mms6 and Mms6C25 bind to pre-made MNPs differently, when immobilized onto gold surfaces.[33] These results indicate that the deficiency of the hydrophobic packing ability in the Mms6C25 peptide not only makes Mms6C25 micelles less stable but also, more importantly, disables its C-terminal DEEVE motif from arranging into the correct packing and orientation that are crucial for protein–crystal recognition. Our RTCP synthesis in the presence of full-length Mms6 produced larger sized magnetite than that in the presence of Mms6C25, suggesting this extended array of DEEVE surfaces from Mms6 micelles may contribute to magnetite nucleation and crystal growth.

Compared to magnetosome magnetite (50 nm in size), smaller magnetite crystals (28 nm in average in our case) were obtained during chemical synthesis in the presence of Mms6 whose micelle size is around 30 nm as shown in Fig. 1c. On an extended surface from immobilized Mms6, larger magnetite particles at size over 70 nm can be obtained as reported by different groups.[19,33,39,40] Many detailed physical and chemical factors from these systems clearly affect the nucleation and crystal growth; nevertheless, the Mms6 surface, which also varies from system to system, plays a more important role by matching to the crystal surface. In our NMR titration study, the Mms6 assembly experiences a transition (as shown in the schematic model in Fig. 5) from small protein micelles (10 nm in the presence of 14 mM DHPC) to extended Mms6 surfaces matching magnetosome magnetite crystal. The global curvature changes which have been proposed to determine the Mms6 surface expansion[18,33,40] and the possible local conformation rearrangement may explain the NMR chemical shift perturbations in Mms6 C-terminal residues after the DEEVE motif.

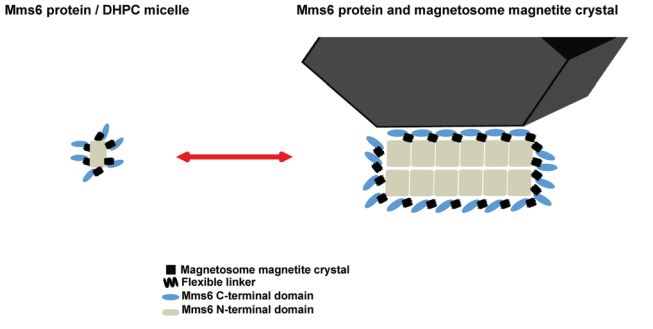

Fig. 5 A schematic assembly model of Mms6 protein micelles before and after magnetosome magnetite crystal binding.

4 Conclusions

The Mms6 protein from *Magnetotactic bacteria* strain AMB-1 is responsible for controlling the formation of magnetite nanoparticles *in vitro* and *in vivo*. Using the high-resolution NMR technique, we are able to study the conformation and self-assembly of Mms6 in aqueous solution. Mms6 self-assembles into protein micelles with the N-terminal domains packed into a hydrophobic core and the C-terminal domains exposed to an aqueous environment. The cytoplasmic domain of the full-length Mms6 protein within the protein aggregates shares similar structural features to the Mms6C25 peptide. Both Mms6 and Mms6C25 are capable of binding to magnetosome nanocrystals. The NMR data of full-length Mms6 protein showed the C-terminal DEEVE motif and residues after adopting conformation change upon magnetosome Fe_3O_4 crystal binding. This observation provided direct evidence for the generally accepted roles of this region in crystal surface recognition and nucleation regulation. The deficiency of the hydrophobic packing ability in the Mms6C25 peptide disables the C-terminal DEEVE motif from arranging into a correct assembly and orientation that are crucial for protein–crystal recognition. Our studies on Mms6 and magnetosome MNPs demonstrate that the high-resolution NMR technique we used can be applied to characterize the interaction details between protein and inorganic crystals in other biomineralization systems.

Acknowledgements

We would like to thank Dr Jinping Xin for TEM measurements and thoughtful discussions. This study was supported by the National Natural Science Foundation of China (Grants U1532269, U1332142, 21372222 and 31070665).

Notes and references

1 B. Devouard, M. Posfai, X. Hua, D. A. Bazylinski, R. B. Frankel and P. R. Buseck, *Am. Mineral.*, 1998, **83**, 1387–1398.
2 A. Arakaki, K. Shimizu, M. Oda, T. Sakamoto, T. Nishimura and T. Kato, *Org. Biomol. Chem.*, 2015, **13**, 974–989.
3 A.-W. Xu, Y. Ma and H. Cölfen, *J. Mater. Chem.*, 2007, **17**, 415–449.
4 C.-Y. Chiu, L. Ruan and Y. Huang, *Chem. Soc. Rev.*, 2013, **42**, 2512–2527.
5 L. Addadi, A. Gal, D. Faivre, A. Scheffel and S. Weiner, *Isr. J. Chem.*, 2015, **56**, 227–241.
6 C. Jimenez-Lopez, C. S. Romanek and D. A. Bazylinski, *J. Geophys. Res.: Biogeosci.*, 2010, **115**, G00G03, DOI: 10.1029/2009JG001152.
7 A. Komeili, *FEMS Microbiol. Rev.*, 2012, **36**, 232–255.
8 T. Matsunaga, Y. Okamura and T. Tanaka, *J. Mater. Chem.*, 2004, **14**, 2099–2105.
9 L. Yan, S. Zhang, P. Chen, H. Liu, H. Yin and H. Li, *Microbiol. Res.*, 2012, **167**, 507–519.
10 A. Arakaki, J. Webb and T. Matsunaga, *J. Biol. Chem.*, 2003, **278**, 8745–8750.
11 M. Tanaka, E. Mazuyama, A. Arakaki and T. Matsunaga, *J. Biol. Chem.*, 2011, **286**, 6386–6392.
12 S. S. Staniland and A. E. Rawlings, *Biochem. Soc. Trans.*, 2016, **44**, 883–890.
13 A. Arakaki, A. Yamagishi, A. Fukuyo, M. Tanaka and T. Matsunaga, *Mol. Microbiol.*, 2014, **93**, 554–567.
14 Y. Amemiya, A. Arakaki, S. S. Staniland, T. Tanaka and T. Matsunaga, *Biomaterials*, 2007, **28**, 5381–5389.
15 T. Prozorov, S. K. Mallapragada, B. Narasimhan, L. Wang, P. Palo, M. Nilsen-Hamilton, T. J. Williams, D. A. Bazylinski, R. Prozorov and P. C. Canfield, *Adv. Funct. Mater.*, 2007, **17**, 951–957.
16 A. Arakaki, F. Masuda, Y. Amemiya, T. Tanaka and T. Matsunaga, *J. Colloid Interface Sci.*, 2010, **343**, 65–70.
17 J. M. Galloway, A. Arakaki, F. Masuda, T. Tanaka, T. Matsunaga and S. S. Staniland, *J. Mater. Chem.*, 2011, **21**, 15244–15254.
18 S. Nayak, H. Zhang, X. Liu, S. Feng, P. Palo, M. Nilsen-Hamilton, M. Akinc and S. Mallapragada, *RSC Adv.*, 2016, **6**, 57048–57056.
19 J. M. Galloway, J. P. Bramble, A. E. Rawlings, G. Burnell, S. D. Evans and S. S. Staniland, *Small*, 2012, **8**, 204–208.
20 L. Wang, T. Prozorov, P. E. Palo, X. Liu, D. Vaknin, R. Prozorov, S. Mallapragada and M. Nilsen-Hamilton, *Biomacromolecules*, 2011, **13**, 98–105.
21 S. Feng, L. Wang, P. Palo, X. Liu, S. K. Mallapragada and M. Nilsen-Hamilton, *Int. J. Mol. Sci.*, 2013, **14**, 14594–14606.
22 H. Zhang, X. Liu, S. Feng, W. Wang, K. Schmidt-Rohr, M. Akinc, M. Nilsen-Hamilton, D. Vaknin and S. Mallapragada, *Langmuir*, 2015, **31**, 2818–2825.
23 S. Kashyap, T. J. Woehl, X. Liu, S. K. Mallapragada and T. Prozorov, *ACS Nano*, 2014, **8**, 9097–9106.
24 G. Mirabello, J. J. Lenders and N. A. Sommerdijk, *Chem. Soc. Rev.*, 2016, **45**, 5085–5106.
25 Z. Oestreicher, E. Mumper, C. Gassman, D. A. Bazylinski, S. K. Lower and B. H. Lower, *J. Mater. Res.*, 2016, **31**, 527–535.
26 T. Prozorov, P. Palo, L. Wang, M. Nilsen-Hamilton, D. Jones, D. Orr, S. K. Mallapragada, B. Narasimhan, P. C. Canfield and R. Prozorov, *ACS Nano*, 2007, **1**, 228–233.
27 A. Wolff, K. Frese, M. Wißbrock, K. Eckstädt, I. Ennen, W. Hetaba, S. Löffler, A. Regtmeier, P. Thomas and N. Sewald, *J. Nanopart. Res.*, 2012, **14**, 1161.
28 A. E. Rawlings, J. P. Bramble, A. M. Hounslow, M. P. Williamson, A. E. Monnington, D. J. Cooke and S. S. Staniland, *Chem. – Eur. J.*, 2016, **22**, 7885–7894.
29 E. Alphandery, S. Faure, O. Seksek, F. o. Guyot and I. Chebbi, *ACS Nano*, 2011, **5**, 6279–6296.
30 E. Alphandéry, F. Guyot and I. Chebbi, *Int. J. Pharm.*, 2012, **434**, 444–452.
31 J. J. Lenders, C. L. Altan, P. H. Bomans, A. Arakaki, S. Bucak, G. de With and N. A. Sommerdijk, *Cryst. Growth Des.*, 2014, **14**, 5561–5568.
32 J. J. Lenders, H. R. Zope, A. Yamagishi, P. H. Bomans, A. Arakaki, A. Kros, G. de With and N. A. Sommerdijk, *Adv. Funct. Mater.*, 2015, **25**, 711–719.
33 S. M. Bird, A. E. Rawlings, J. M. Galloway and S. S. Staniland, *RSC Adv.*, 2016, **6**, 7356–7363.

34 P. Bayer, A. Arndt, S. Metzger, R. Mahajan, F. Melchior, R. Jaenicke and J. Becker, *J. Mol. Biol.*, 1998, **280**, 275–286.
35 J. R. Schnell and J. J. Chou, *Nature*, 2008, **451**, 591–595.
36 J. Wang, R. M. Pielak, M. A. McClintock and J. J. Chou, *Nat. Struct. Mol. Biol.*, 2009, **16**, 1267–1271.
37 A. M. Seddon, P. Curnow and P. J. Booth, *Biochim. Biophys. Acta, Biomembr.*, 2004, **1666**, 105–117.
38 J. Baumgartner, A. Dey, P. H. Bomans, C. Le Coadou, P. Fratzl, N. A. Sommerdijk and D. Faivre, *Nat. Mater.*, 2013, **12**, 310–314.
39 S. M. Bird, J. M. Galloway, A. E. Rawlings, J. P. Bramble and S. S. Staniland, *Nanoscale*, 2015, **7**, 7340–7351.
40 X. Liu, H. Zhang, S. Nayak, G. Parada, J. Anderegg, S. Feng, M. Nilsen-Hamilton, M. Akinc and S. K. Mallapragada, *Ind. Eng. Chem. Res.*, 2015, **54**, 10284–10292.